

PACS numbers: 42.65.Jx; 42.68.Ay; 52.50.Jm
DOI: 10.1070/QE2014v044n05ABEH015427

Influence of the laser beam size on the length of a filament formed by high-power femtosecond laser radiation in air

Yu.E. Geints, S.S. Golik, A.A. Zemlyanov, A.M. Kabanov, G.G. Matvienko

Abstract. **The single-filamentation regime of GW femtosecond laser beams of millimetre diameter, propagating in atmospheric air under collimated and tight focusing, has been theoretically and experimentally (at wavelengths of 800 and 400 nm) investigated. The influence of the initial size of the light beam on the spatial characteristics of the filamentation region is systematically analysed. The filamentation length for collimated beams with the same initial power is found to nonmonotonically depend on the initial beam radius. In this case, the filament start point is displaced, and the longitudinal continuity of the related plasma channel is lost. For tightly focused beams, the observed filament length barely depends of the initial beam radius, provided that the peak intensity remains constant.**

Keywords: *self-focusing, filamentation, femtosecond laser radiation.*

1. Introduction

Self-focusing and filamentation are the brightest and largest scale effects, which accompany the propagation of high-power ultrashort laser pulses in cubically nonlinear media, such as air, water and quartz. They have been intensively investigated for more than 50 years (see, for example, reviews [1–4] and references therein). Along with many practical applications (broadband lidar sensing, formation of conducting channels, transfer of high-intensity radiation at large distances, frequency conversion, etc.), these effects are also interesting from the fundamental point of view, because they significantly expand the potential of nonlinear optics and physics of superstrong fields.

Filamentation of a laser beam propagating in a medium experimentally manifests itself as a thin luminous filament, which visualises the beam path. The initial cause of filamentation is the cubic polarisability of the medium (Kerr-type nonlinearity), which gives rise to a self-induced increase in the refractive index in the regions of enhanced radiation intensity and subsequent progressive transverse compression of the laser beam with a power sufficient for this compression (i.e., self-focusing). The beam collapse into a line is restricted by a number of physical mechanisms, among which photoionisation and plasma formation dominate in the case of a gas medium. The result of the dynamic balance between the diffraction, self-focusing and plasma nonlinearity is a set of spatially localised high-intensity light structures, i.e., filaments; they are formed in the beam and are retained on a rather long segment of the beam path.

A unique property of filaments is the absence of any significant dependence of their main characteristics (transverse size and peak intensity) on the initial beam size. It has been proved in numerous studies that the main properties of an individual filament are mainly determined by the lasing wavelength and the optical characteristics of the propagation medium [3, 4].

The situation with the filament length, i.e., the distance at which the luminous filament and beam energy channelling are observed, is different. Paradoxical as it may seem, this characteristic (which is undoubtedly important) has been rather poorly studied. Despite the fact that the filamentation of beams of different sizes was modelled and experimentally studied in some studies [1], specific dependences of the filamentation region parameters on the beam radius were not reported. At the same time, this question is very important for developing models of atmospheric propagation of wide-aperture ultrashort beams, which are generally implemented in the multiple-filamentation regime.

Concerning the single-filamentation regime (the subject of our further consideration), it is intuitively clear that the filament length should be determined by the loss of the total beam energy spent on the formation of an ionised channel. This direct energy loss must be supplemented with the so-called extra loss on the conversion of the fundamental frequency to the supercontinuum radiation and on the Rayleigh scattering from plasma microaggregates [5]. Then, provided that the single-filament parameters are independent of the beam size, the filament length should also be invariant to the initial beam radius and depend only on its energy (power) [6]. Below we will dwell on this question and show that this does not always hold true.

One of the factors leading to the dependence of the filament length on the beam radius is the violation of filament longitudinal continuity, which is observed for light beams with powers greatly exceeding the critical value [7]. The filament becomes intermittent (composed of several shorter unbounded fragments); this intermittence is due to multiple beam refocusings and longitudinal filament instability (caused by the increasing effect of diffraction on the beam axis). Obviously, this effect should be enhanced with an increase in the beam radius and may influence the total filamentation length; however, there are no specific estimates and calculations of this effect to the best of our knowledge.

Yu.E. Geints, A.A. Zemlyanov, A.M. Kabanov, G.G. Matvienko
V.E. Zuev Institute of Atmospheric Optics, Siberian Branch, Russian Academy of Sciences, pl. Akad. Zueva 1, 634021 Tomsk, Russia;
e-mail: ygeints@iao.ru;
S.S. Golik Far Eastern Federal University, ul. Sukhanova 8, 690950 Vladivostok, Russia

Received 3 March 2014; revision received 21 March 2014
Kvantovaya Elektronika **44** (5) 489–497 (2014)
Translated by Yu.P. Sin'kov

All the aforesaid is mainly related to the filamentation of collimated or weakly focused beams. At the same time, spatial (external) beam focusing adds some new features to the process of formation of filaments and to their spatial characteristics. The most characteristic among these features is the decrease in the filament length and limitation of its far boundary by the beam focal waist. The manifestation of this effect turned out to depend on both the initial laser pulse power and the beam focusing sharpness [8], as well as on the filamentation type (single or multiple) [9].

In this study we consider one of the aspects of filamentation, which is related to the influence of the initial beam size. First, we will use numerical simulation to show that the main characteristics of filaments (starting coordinate, length and continuity) depend on the beam radius (provided that the initial beam power is constant) for collimated beams of millimetre diameter in the single-filamentation regime. The filament start point begins to move apart from the beginning of the path, and the total filament length nonmonotonically depends on the beam diameter, first increasing with an increase in the diameter and then virtually vanishing (a situation corresponding to complete termination of filamentation) for relatively wide beams (more than 4 mm in diameter).

Then we report the results of our laboratory experiments on self-focusing and filamentation of a previously tightly focused femtosecond laser beam in air under conditions of changing its initial size and power. In particular, to the best of our knowledge, experimental data indicative of extremely weak dependence (almost invariance) of the filament length of laser beam on its radius [when the peak intensity (not power!) remains constant] are published for the first time. This result is not a direct consequence of the theory of light self-focusing and differs significantly from the properties observed for collimated-beam filamentation.

2. Theoretical model

Our numerical experiments were based on solving the quasi-optics equation for the complex envelope of a light-wave electric field strength $E(\boldsymbol{r}_\perp, z, t)$, with allowance for the nonlinearity of the medium; this equation is referred to as the nonlinear Schrödinger equation. The model of air optical nonlinearity included both instantaneous and inertial Kerr components, higher order nonlinearity (saturation of Kerr nonlinearity), and the change in the complex refractive index of the medium due to the photoionisation of air molecules and formation of free-electron gas. The linear part of the equation described the group-velocity dispersion of the laser pulse and the beam diffraction. The dynamics of free-electron density ρ_e in the beam channel was calculated using the corresponding rate equation, which takes into account the combined (multiphoton and tunnel) mechanism of ionisation of atoms of atmospheric air components (nitrogen and oxygen).

The wave envelope propagation equation in the coordinate system related to a pulse moving with a group velocity has the form

$$\left(\frac{\partial}{\partial z} - \frac{\mathrm{i}}{2n_0k_0}\nabla_\perp^2 + \mathrm{i}\frac{k''_\omega}{2}\frac{\partial^2}{\partial t^2}\right)U =$$

$$\mathrm{i}k_0(n'_2 + n_{\mathrm{HOKE}} + n_{\mathrm{pl}})U - \alpha_{\mathrm{NL}}U. \qquad (1)$$

The plasma free-electron density $\rho_e(\boldsymbol{r}_\perp, z, t)$ is given by the rate equation

$$\frac{\partial\rho_e}{\partial t} = \Psi_i(I)(\rho_n - \rho_e). \qquad (2)$$

Here, $U = E/E_0$ is the field amplitude normalised to the initial value; n_0 is the linear refractive index of the medium; $k_0 = 2\pi/\lambda_0$ is the wave number; λ_0 is the radiation carrier wavelength; $I = cn_0|U|^2/(8\pi)$ is the radiation intensity; c is the speed of light in vacuum; $k''_\omega = \partial^2 k/\partial\omega^2$ is the second-order dispersion coefficient of the light-pulse group velocity in the medium;

$$n'_2 = \frac{n_2}{2}\left\{\int_{-\infty}^{t}[\delta(t) + \Lambda(t-t')]|U(t')|^2\mathrm{d}t'\right\}$$

is the cubic (Kerr) nonlinearity coefficient; $n_{\mathrm{HOKE}} = \sum_{m=2}^{M} n_{2m}I^m$ is the high-order Kerr effect nonlinearity; n_{2m} is the nonlinear additive to the refractive index, which is due to the nonlinear susceptibility of the medium of the $(2m+1)$th order; $\delta(t)$ is the Dirac delta function; $\Lambda(t)$ is a dimensionless function of time, which takes into account the inertial component of the cubic response of the medium to the light field; $n_{\mathrm{pl}} = -\rho_e/(2\rho_c n_0)$ is the coefficient of 'plasma' nonlinearity; $\rho_c = \omega_0^2 m_e/e^2$ is the critical plasma electron density; m_e is the electron rest mass; e is the elementary charge; Ψ_i is the photoionisation probability for a gas with a concentration of neutral atoms (molecules) ρ_n; ω_0 is the centre radiation frequency; $\alpha_{\mathrm{NL}} = \sigma_c\rho_e/2 + (2I)^{-1}[\Psi_i\Delta E_i(\rho_n - \rho_e)]$ is the nonlinear absorption coefficient of the medium; and σ_c and ΔE_i are, respectively, the shock ionisation cross section and the atomic ionisation potential.

The Kerr nonlinearity inertia, which is related to the rotational stimulated Raman scattering of a light wave from air molecules, was taken into account within the damping oscillator model: $\Lambda(t) = \theta(t)\Omega_R\exp(-t/\tau_d)\sin\Omega_R t$, where the air molecule oscillation frequency is $\Omega_R = 20$ THz, the characteristic damping time is $\tau_d = 70$ fs, and $\theta(t)$ is the Heaviside function. For the radiation wavelength $\lambda_0 = 800$ nm, the coefficients in Eqns (1) and (2) were chosen to be as follows: the nonlinear refractive index of the medium $n_2 = 3.0\times10^{-23}$ m^2 W^{-1}, the number of retained terms in the expression for the higher nonlinearities is $M = 4$ (in correspondence with the experimental data of [10]), and the group velocity dispersion $k''_\omega = 0.21$ fs^2 cm^{-1}. For the second harmonic ($\lambda_0 = 400$ nm), $n_2 = 5.4\times10^{-23}$ m^2 W^{-1}, $n_{\mathrm{HOKE}} = 0$, and $k''_\omega = 0.81$ fs^2 cm^{-1}. The other parameters were taken to be $\sigma_c = 5.52\times10^{-24}$ m^2 and $\Delta E_i = 12.1$ eV (for oxygen). The critical self-focusing power [$P_c = \lambda_0/(n_0k_0n_2)$], with allowance for only the instantaneous component of Kerr nonlinearity, is 3.2 GW for the fundamental harmonic and 0.5 GW for the second harmonic [11]. The photoionisation rate of gas-medium atoms, Ψ_i, was calculated within the Perelomov–Popov–Terent'ev ionisation model [12].

The space–time distribution of the light-pulse normalised amplitude in the beginning of the path was set in the form of a Gaussian:

$$U(\boldsymbol{r}_\perp, z = 0; t) =$$

$$\exp\{-|\boldsymbol{r}_\perp|^2[1/(2R_0^2) + \mathrm{i}k_0/(2f)]\}\exp[-t^2/(2t_p^2)], \qquad (3)$$

where $|\boldsymbol{r}_\perp| = \sqrt{x^2+y^2}$; t_p is the pulse width (was taken to be 100 fs in the calculations), and f is the focal length of the optical system. To provide the single-filamentation conditions for the beam, the pulse peak pulse P_0 was limited from above by the value $10P_c$. In addition, we did not consider beams with radii more than 5 mm for the following reason: such beams

are likely to undergo multiple filamentation under real conditions because of the modulation instability of Kerr self-focusing.

3. Filamentation of collimated beams

Figure 1 shows the numerically calculated evolution of the radius R_w of a collimated ($f \to \infty$) light beam, determined from the energy density profile $w(\boldsymbol{r}_\perp)$ as the 1/e half-width; actually, this parameter is the light-filament radius. Figure 1 presents also the dependence of the peak free-electron density ρ_{em}, which characterises the plasma formed in the channel. The dependences were calculated for a constant initial laser beam power and varied initial beam radius. Note that the propagation coordinate is normalised to the Rayleigh beam length $L_R = k_0 R_0^2/2$ (calculated for the corresponding beam radius R_0) and the peak pulse power is reduced to the critical value: $\eta = P_0/P_c$.

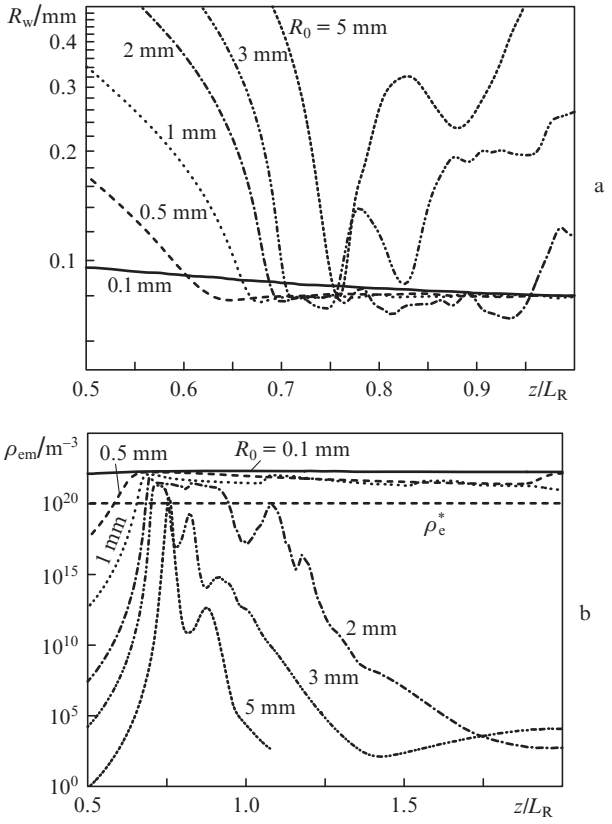

Figure 1. Evolution of the (a) collimated-beam radius and (b) the peak free-electron density along the beam path during self-focusing in air for beams with $\eta = 5$ and different initial radii R_0.

It can be seen that beams of different sizes propagate along the path in a similar way; their behaviour is determined by different stages of radiation self-action. First, the self-focusing caused by the cubic nonlinearity of the medium leads to transverse compression of the beam, a decrease in R_w, and a rise in ρ_{em}. The next path fragment corresponds to the beam filamentation and plasma channel formation. The beam broadening after this fragment, with a simultaneous decrease in the plasma density, suggests temporal or final termination of the filament at this point.

Let us first consider the start point z_s of the filament. The beginning of the filamentation region is determined proceeding from the balance of self-focusing and diffraction effects [13]. It is generally accepted to use the Marburger formula [14] to estimate the coordinate of the filamentation start point for a collimated laser beam in the theory of time-dependent self-focusing of light pulses. This formula (obtained by approximating a large amount of calculation data) explicitly contains the initial parameters of laser radiation and is written in the form

$$z_s(\eta) = \frac{0.367 L_d}{\sqrt{(\sqrt{\eta} - 0.852)^2 - 0.0219}}, \qquad (4)$$

where $L_d = 2L_R$ is the characteristic diffraction length. Obviously, this expression is valid only at $\eta > 1$.

If we use the dimensionless coordinate z_s/L_R in (4), this expression becomes independent of the light-beam radius R_0. Therefore, at a constant relative power η, the filament should start at the same point in the normalised coordinates. At the same time, the plots in Fig. 1 contradict this statement: with an increase in the beam radius the filament start point shifts to the end of the path (at a rather large distance).

Figure 2 shows the dependence of the parameter z_s/L_R on the beam radius; this parameter was determined by numerical simulation, provided that the peak free-electron density ρ_{em} on the beam axis exceeds the specified concentration $\rho_e^* = 10^{20}$ m^{-3}. The calculation was performed for a discrete set of beam radii; for clarity, the calculation points are connected by a spline approximation curve. It can be seen that this dependence can be described fairly well by a fractional-power-law: the coordinate changes with a change in R_0 for narrow beams ($R_0 < 1$ mm), whereas for relatively wide beams the displacement of the filament start point is less pronounced.

We intentionally omitted the ratio z_s/L_R calculated from formula (4) in Fig. 2, because Eqns (1) and (2) were numerically solved using the complete model of air optical nonlinearity, which includes the inertia in time and saturation of the cubic response of the medium, whereas these factors are disre-

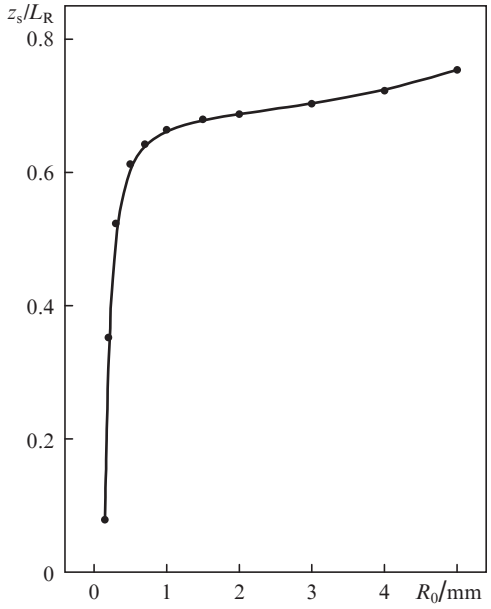

Figure 2. Dependence of the coordinate of the filament start point, z_s/L_R, on the initial beam radius R_0 ($\eta = 5$).

garded in the Marburger formula. However, our calculations for the case of 'pure' Kerr nonlinearity (are also omitted here) showed that the aforementioned behaviour of the parameter z_s/L_R is retained with a change in R_0, while the Marburger formula most exactly predicts the coordinate of the filament start point specifically for wide beams with $R_0 > 2$ mm and relative powers in the range of $1 < \eta < 15$.

Strictly speaking, it is incorrect to expect the Marburger formula to describe exactly the dependence presented in Fig. 2, because expression (4) is for the beam self-focusing length considered as the coordinate of the first singularity or local collapse (in contrast to the entire-beam collapse [15]) in the evolutionary dependence of $R_w(z)$] [14]. Obviously, beams do not collapse in practice. In theory, the self-focusing singularity is removed by taking into account the mechanisms in the optical nonlinearity of the medium that lead to saturation of the pulse intensity via nonlinear (multiphoton) absorption and/or decrease in the cubic nonlinearity coefficient (higher order nonlinearity). In addition, the model can also take into account the compensating effect of the plasma formed in the channel, which reduces the effective value of the nonlinear refractive index of the medium and causes additional beam defocusing. The joint effect of these factors stops the transverse beam collapse at some quasi-equilibrium value of the peak intensity, I_{fil}, which also determines the quasi-equilibrium filament radius R_{fil} for the chosen nonlinearity model [6]. It is important that neither I_{fil} nor R_{fil} (see Fig. 1a) depend on the initial beam radius.

Thus, when light beams with the same initial power but different radii are self-focused in a medium, they can be compressed to only a certain absolute size. Since these beams are transversely compressed with the same relative rate (which is determined only by the parameter η) [15], a wider beam should attain the limiting radius R_{fil} at a larger distance than a beam of smaller radius. If a beam is so narrow that its initial peak intensity $I_0 \geqslant I_{fil}$ at a specified η value, a filament will be formed almost immediately at the input of the medium; then, $z_s \to 0$. Therefore, the filament start point should approach zero with an increase in the laser pulse intensity I_0 or (what is the same) with a decrease in the beam radius R_0. A regression analysis of the functional dependence in Fig. 2 showed its similarity with the dependence $z_s/L_R \propto R_0^{1/6}$.

Recalling Fig. 1, we should note that the amplitude of oscillations of the beam radius and electron density increases with increasing initial beam radius. Indeed, for initially narrow beams, the transverse size of the filament formed is rather stable, which is indicative of the formation of a continuous light channel along the path. However, beginning with $R_0 =$ 2 mm, the filament clearly exhibits regions of significant expansion and then (if the filament boundary is assumed to correspond to $\rho_{em} = 10^{20}$ m^{-3}) is either interrupted or recovered again. In other words, the longitudinal intermittence of filamentation develops with an increase in the initial beam radius. This effect has been described in the literature; it is often related to the so-called successive light beam refocusing in a Kerr medium [7].

The properties revealed are mainly due to the fact that a wider beam is subjected to stronger transverse compression in the initial portion of the path due to the self-focusing. The 'inlet' angle of diffracted rays into the filament start point z_s (nonlinear focus) for a beam with, for example, $R_0 = 3$ mm is much larger than the corresponding angle for a narrow beam. Therefore, the diffraction efficiency of wide beams is higher. Along with the plasma defocusing, the diffraction mechanism 'bounces' rays from the nonlinear focus, due to which the filament rapidly terminates. In essence, this effect is similar to the decrease in the filament length that occurs with an increase in the curvature of the initial-beam phase front after passing through an optical focuser [16, 17].

The compression of a narrow beam during self-focusing is much smaller because of the higher initial intensity; it affects mainly the axial region. The other rays at the beam periphery begin almost immediately to diverge stably. Calculations show that the angular divergence of a narrow beam directly after the nonlinear focus, determined from the rms radius [18], is an order of magnitude smaller than the wide-beam divergence.

The second and subsequent filamentation portions for a wide beam (Fig. 1b, $R_0 = 3$ mm) arise for the following reason: at a sufficient excess power ($\eta \gg 1$), some rays from the energy environment of the filament become negatively divergent due to the Kerr effect after the filament termination. These rays start converging to the optical axis, 'pressing' the axial rays and preventing light energy escape from the filament. Thus, favourable filamentation conditions are implemented again.

Let us now consider how the filament length depends on the light-beam size. Primarily, we should specify that the filament length is assumed to be equal to the total length of the optical path segment beginning at the filamentation start point z_s and ending at the point with the farthest coordinate z_e, corresponding to the filament termination. This coordinate was calculated proceeding from the profile of peak free-electron density $\rho_{em}(z)$ as the extreme point at which ρ_{em} is reduced to a concentration below ρ_e^*, i.e., $\rho_{em}(z > z_e) < \rho_e^*$ (see Fig. 1b). The results of these calculations in the form of the dependence of the filament length L_{fil} on the light-beam radius for two powers are shown in Fig. 3.

The curves in Fig. 3a indicate that the filament length normalised to the Rayleigh length monotonically decreases with light beam expansion both at $\eta = 5$ and at the doubled η value. Only beams with millimetre diameter (and narrower ones) yield a filament length exceeding L_R. As follows from the previous consideration, these filaments are characterised by longitudinal continuity.

It is of interest that the aforementioned decrease in the filament length with an increase in the beam size is not caused by the increased energy loss. On the contrary, as our analysis shows, the wider the beam, the lower its loss on filamentation. Even in the 'worst' case (a narrow beam with $R_0 = 200$ μm), the total energy loss does not exceed 20%.

The dependence $L_{fil}(R_0)$ in Fig. 3b exhibits an extremum in the range of beam radii $R_0 \approx 0.8–1.5$ mm. In narrower beams the decrease in the filament length is due to the quadratic dependence of the Rayleigh length on R_0. In wider beams the decrease in the filament length is related to the filament intermittence. In this case, despite the oscillations of the beam radius caused by successive beam refocusings, the peak electron density after the initial filamentation segment remains close to the threshold concentration ρ_e^* (see, for example, curves for $R_0 = 3$ and 5 mm in Fig. 1b), and there is no filamentation.

A filament can be initiated in the refocusing zones only by increasing the initial laser pulse power. As can be seen in Fig. 3, this procedure increases the total filament length, and this effect is most pronounced for specifically wide beams.

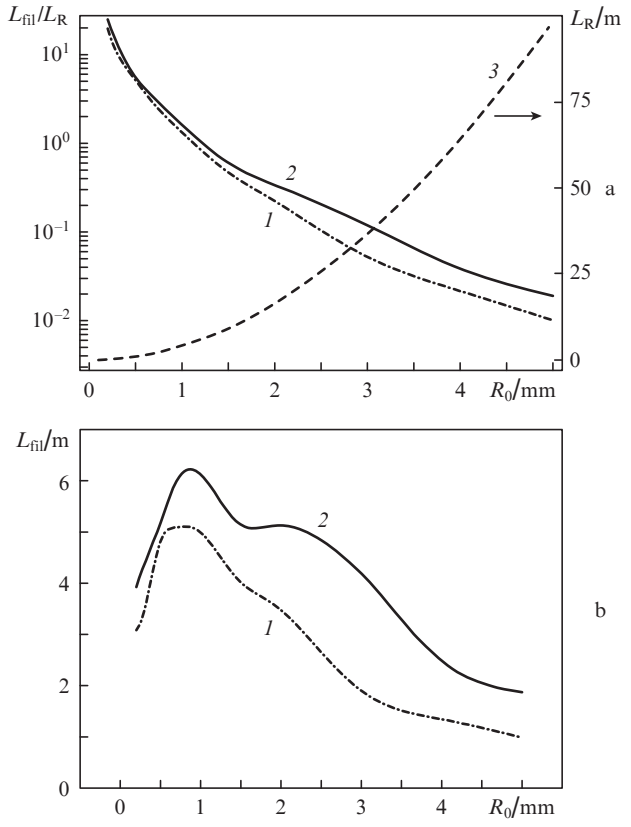

Figure 3. (a) Filament length normalised to the Rayleigh length and (b) the dimensional filament length for beams with different initial radii and relative powers η = (*1*) 5 and (*2*) 10. Curve (*3*) is the Rayleigh beam length.

4. Filamentation of tightly focused beams

We performed experiments on self-focusing and filamentation of focused radiation using a pulsed Ti:sapphire laser beam at wavelengths of the fundamental (800 nm) and second (400 nm) harmonics, with a width of 45 fs and gigawatt power. The experimental bench is schematically shown in Fig. 4.

The technique for measuring the size parameters of plasma filaments was described in detail in [19]. We employed laser beams with diameters d_0 = 2.5, 4.5, and 9 mm. The 4.5-mm beam was formed from the initial beam 9 mm in diameter using a telescope, in which the sequence of lenses was changed to obtain narrower beams, with the same telescope base D, corresponding to the collimated beam at the telescope output. A beam 2.5 mm in diameter was cut by a diaphragm from the initial beam. The data on the spatial characteristics of the filaments formed as a result of focusing 7-mm beams were taken from [19].

The beam energy and profile were measured after the beam passage through the telescope or diaphragm before the focusing lens. Plasma filaments were recorded at identical values of the laser pulse energy and power for beams of different diameters.

Our main purpose was to gain information about the dependence of the filament length and position on the initial beam size for a tightly focused femtosecond laser beam. To this end, the filamentation region was recorded by a CCD camera from aside, near the geometric focus of the lens. The light emission during filamentation is known [20] to be caused by the formation of a plasma in the beam channel and by the fluorescence of nitrogen molecules, excited as a result of ionisation by the intense optical field of the laser pulse; thus, this luminescence can be considered as an indicator of beam filamentation. The fluorescence brightness is proportional to the number of free electrons formed during the laser pulse in the beam channel as a result of ionisation of gas molecules. Images of filamentation regions for beams of different sizes and two harmonics of Ti:sapphire laser radiation, recorded near the lens focus, are shown in Figs 5a–5d. The linear sizes of each frame are 60×8 mm.

The images in Figs 5a–5d show a tendency to a decrease in the filamentation length with increasing light beam diameter d_0 at a constant initial power P_0. This tendency is observed for both spectral ranges of the radiation. In addition, an increase in the beam size leads to an increase in its transverse size (width) and brightness of the luminescence region; the latter shifts toward the geometric focus of the lens. Note that the peak power for both the fundamental and second harmonics multiply exceeds the threshold self-focusing power in air.

The experimental data on the filament length L_{fil} at different radiation powers are presented in Fig. 6. According to these data, the filament length monotonically increases with an increase in the laser pulse power and reaches ~5 cm for the narrowest beam used by us. The slope of the dependence $L_{fil}(P_0)$ decreases with an increase in the light-beam size; for the widest beam (d_0 = 9 mm), L_{fil} changes only slightly with an increase in P_0.

We will interpret the characteristi features obtained in the framework of the theory of stationary self-focusing of light in

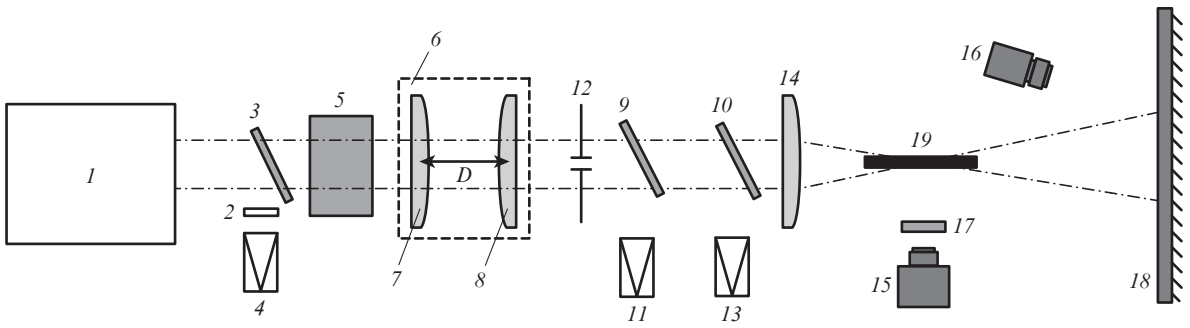

Figure 4. Scheme of the experiments: (*1*) laser source; (*2*) attenuator; (*3*, *9*, *10*) rotational plates; (*4*) autocorrelator; (*5*) β-BaB_2O_4 harmonic converter; (*6*) telescope; (*7*, *8*) lens; (*11*) energy meter; (*12*) diaphragm with a diameter d_0 = 2.5 mm; (*13*) beam profile meter; (*14*) focusing lens (f = 200 mm); (*15*) CCD camera; (*16*) photo camera; (*17*) linear polariser; (*18*) screen; (*19*) filamentation region.

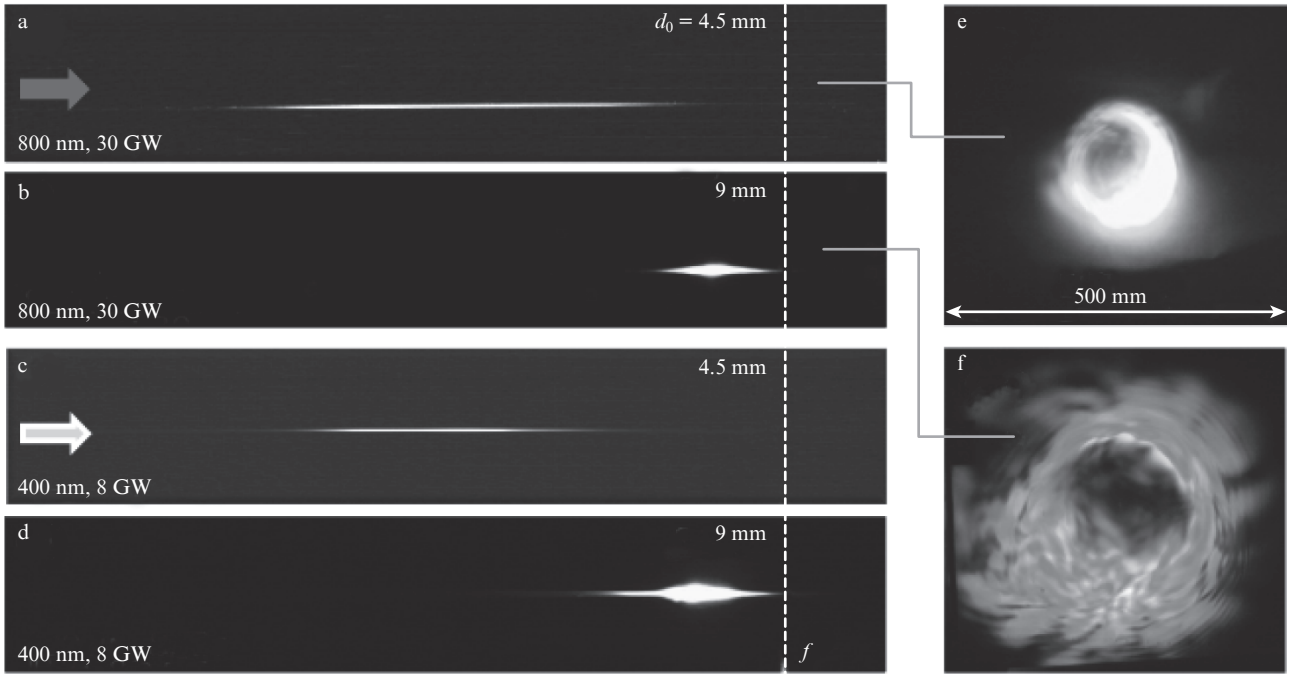

Figure 5. (a–d) Filament luminescence images for two radiation wavelengths at different initial diameters and peak powers of the laser beam (the vertical dashed line corresponds to the geometric focus) and the images of the transverse profile of laser beams with d_0 = (e) 4.5 and (f) 9 mm on a screen.

a Kerr medium [13, 15]. The rms (effective) radius R_e of a beam propagating in such a medium, with allowance for the effects of cubic nonlinearity and external focusing, obeys the following evolution law

$$R_e^2(z) = (1-\eta)(\theta_d z)^2 + R_e^2(0)(1 - z/f)^2\,, \qquad (5)$$

where parameter θ_d is the natural diffraction divergence of the laser beam. For a Gaussian beam in the aberration-free approximation, $R_e \equiv R_0$ and $\theta_d = 1/(k_0 R_0)$. This law is valid only at $\eta > 1$ and predicts a transverse collapse of the beam as a whole at the point $z_{cf} = f/(1 + f/z_c)$, where $z_c = L_d/\sqrt{\eta - 1}$, and $L_d = R_0/\theta_d$.

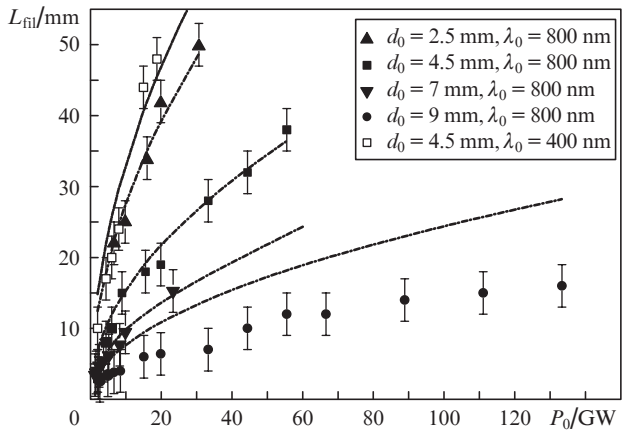

Figure 6. Dependences of the filament length on the peak radiation power at different wavelengths λ_0 and beam diameters d_0 (symbols). The curves are the result of approximation according to formula (8).

In the first approximation we assume that this coordinate corresponds to the filament start point, $z_s = z_{cf}$, and relate the filament end, in correspondence with Fig. 6, with the middle of the beam focal waist, $z_s = z_{cf}$. Then the expression for the filament length L_{fil} is written in the form

$$L_{fil} \equiv f - z_{cf} \approx f^2\sqrt{\eta - 1}/L_d\,, \qquad (6)$$

which takes into account the tight-focusing condition: $f \ll z_c, L_d$. The structure of expression (6) indicates a functional relationship between the filament length and the laser beam parameters: $L_{fil} \propto \lambda_0 R_0^{-2} P_0^{1/2} P_c^{-1/2}$.

With allowance for the dispersion dependence of the critical power, which can roughly be considered proportional to the fourth power of the radiation wavelength, $P_c \propto \lambda_0^4$ [21, 22], we finally arrive at

$$L_{fil} \propto \lambda_0^{-1} R_0^{-2} P_0^{1/2}. \qquad (7)$$

It follows from (7) that, all other factors being equal, the filament length should increase proportionally to the squared root of the initial beam power. In addition, the length L_{fil} increases quadratically with a decrease in the beam radius at a constant power and should be inversely proportional to the radiation wavelength.

An analysis of the plots in Fig. 6 shows that the functional dependence $L_{fil} \propto \sqrt{P_0}$ is satisfied fairly exactly. The comparison of the filament lengths at the same peak pulse power for both harmonics also yields their inverse proportionality to the wavelength, i.e., $L_{fil} \propto 1/\lambda_0$. At the same time, the inverse quadratic dependence of L_{fil} on the beam radius (or diameter) R_0 (7) is not observed. In reality, this dependence is weaker: $L_{fil} \propto 1/R_0$. This is evidenced by the approximating curves in Fig. 6, which were calculated from the formula

$$L_{\text{fil}} = A\sqrt{P_0}/d_0, \tag{8}$$

where $A = 22$ is a fitting constant, L_{fil} and d_0 are in millimetres, and P_0 is in gigawatts.

It can be seen that this expression describes with a rather high accuracy the experimental dependences for three beam sizes. The only exception is the widest beam, for which the filament length increases much slower than it should according to formula (8). This property is also observed for the second harmonic (is omitted in Fig. 6). This decrease in the filament length is likely to be caused by the development of optical breakdown in the lens focus, which leads to illumination of the CCD matrix and an error in determining the position of the filament start point.

The much higher density of the plasma formed as a result of filamentation of a wide beam with $d_0 = 9$ mm is indirectly evidenced by the shift of its image in the screen to the blue wavelength range (see Fig. 5f) in comparison with the filamentation region of the narrower beam with $d_0 = 4.5$ mm (Fig. 5d), which is mainly yellow. Indeed, the initially narrow spectrum of the laser beam is transformed into a supercontinuum as a result of its self-phase modulation under the conditions of Kerr effect and plasma formation in the medium. The inertialess Kerr effect provides a symmetric (with respect to the pulse centre frequency) spectral broadening, whereas the plasma is mainly responsible for the rise in the intensity of the short-wavelength wing [1].

The above-established dependence (8) of the filament length on the beam size leads to an important consequence. Having expressed the initial pulse power in terms of its average intensity, $P_0 = (4\pi)^{-1} I_0 d_0^2$, we derive the following relation from (7):

$$L_{\text{fil}} = A'\sqrt{I_0}, \tag{9}$$

where $A' = A\sqrt{\pi}/2$. In other words, tightly focused laser beams with the same average intensity should also have the same filament length, irrespective of their initial size. This fact indeed holds true; it is illustrated in Fig. 7, which also presents a dependence calculated from formula (9). As well as in Fig. 6, the widest beam stands out from the general pattern.

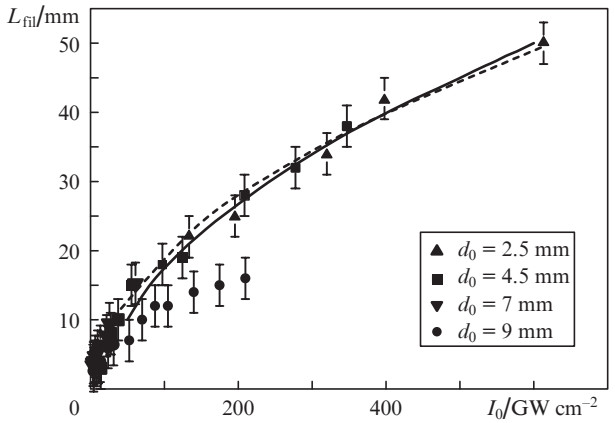

Figure 7. Dependences of the filament length on the peak pulse intensity at different beam diameters d_0 and wavelength $\lambda_0 = 800$ nm (symbols). The dashed line is the result of approximation according to formula (9) and the solid line is the result of numerical calculation.

It should be noted that expression (8) does not stem directly from the stationary self-focusing theory [15], which, as was shown above, predicts the dependence $L_{\text{fil}}(R_0)$ in the form of (7). One might suggest that the discrepancy between the theory and experiment is due to the fact that formula (6) was derived disregarding the beam-profile aberrations during self-focusing in a nonlinear medium. These aberrations are caused by the Kerr nonlinearity, which quadratically depends on the optical-wave amplitude; therefore, it acts differently in the low- and high-intensity beam regions.

To check this hypothesis, we numerically simulated the propagation of high-power laser pulses in air under external focusing. Figure 8 shows the calculated transverse intensity distributions for the femtosecond laser radiation, which were formed prior to the filamentation as a result of the beam propagation in air after focusing ($f = 20$ cm). The profiles of two Gaussian beams with the same initial intensity ($I_0 = 0.25$ TW cm^{-2}) but different diameters d_0 are presented [Fig. 8a, curves (*1*, *2*)]. In the calculations the longitudinal coordinate z_s was considered to be the filament start point when the peak intensity characteristic of filamentation in air, $I_{\max}(r = 0, z_s) = I_{\text{fil}} = 30$ TW cm^{-2}, was reached on the beam axis.

It can be seen that both beams (narrow and wide) practically completely retain the Gaussian intensity profile (at least near the axis); it is also shown in Fig. 8a [curve (*4*)]. This fact

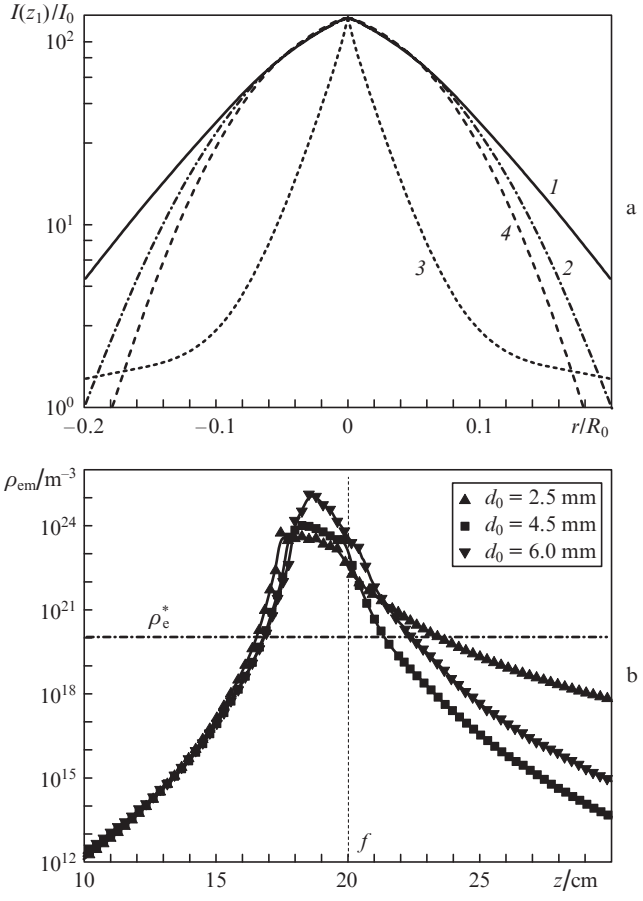

Figure 8. (a) Transverse intensity profiles of (*1*, *2*) focused, (*3*) collimated and (*4*) initial laser beams ($\lambda_0 = 800$ nm, $I_0 = 250$ GW cm^{-2}) at d_0 = (*1*) 1.5 and (*2–4*) 4.5 mm at a distance $z_1 = 18$ cm. (b) Maximum free-electron density on the axis of beams with different diameters in the vicinity of the focal waist.

indicates that the increase in the pulse intensity to the level corresponding to filamentation occurs on the whole in a self-similar way and is accompanied by very small profile distortions. At the same time, the aberrations of a collimated beam with the same initial intensity and size [Fig. 8a, curve (*3*)] can be rather large; they manifest themselves in the elongation of the central part of the beam and formation of a wide background. Obviously, the aberrations during self-focusing of tightly focused radiation does not lead to this effect, and there must be another cause of the experimentally observed regularities.

The fairly small distortions of the profile of a tightly focused beam during self-focusing suggest that the beam propagation to the nonlinear focus is quasi-linear and that the role of the Kerr self-focusing effect by the instant of filamentation onset is insignificant. One can suggest to a certain extent that, under conditions of tight external focusing, a filament arises mainly as a result of this linear beam compression. On the contrary, under soft external focusing, the spatial beam compression is entirely caused by the self-focusing.

Obviously, this does not mean that there is no self-action and filamentation for tightly focused beams propagating in a medium. The case in point is only the initial stage of self-focusing, i.e., the path passed by a beam before its (first) nonlinear focus. The nonlinearity of the medium (of both Kerr and plasma types) is switched on specifically in the close proximity of this focus and continues to act throughout the entire focal waist, leading to phase self-modulation of the laser pulse and providing its filamentation.

Based on the above suggestions about the quasi-linear beam propagation prior the focus, we correct formula (5), i.e., exclude completely nonlinear terms. Then we arrive to a simple expression for the filament length (the tight-focusing condition $f \ll L_d$ is retained):

$$L_{fil} \approx f\sqrt{I_0/I_{fil}}\,. \qquad (10)$$

A comparison of (10) with (9) shows that these expressions are identically accurate to coefficients. The invariance of L_{fil} with respect to the beam radius is satisfied, and the desired wavelength dependence of L_{fil} is introduced through the I_{fil} value [6, 23].

A numerical simulation of the above-considered situation confirms fairly well the experimentally established properties. In particular, Fig. 8b shows the calculated dependences of the axial free-electron density in the plasma formed by the pulse end as a result of air photoionisation on the longitudinal coordinate for three beam sizes at a fixed peak intensity. The filamentation threshold is arbitrarily set to be 10^{20} m^{-3}; it is shown by a horizontal dot-and-dash line in Fig. 8b.

An analysis of these dependences reveals that, as in the experiments, the coordinate of the filament start point barely depends on the beam diameter. The variations in this coordinate do not exceed few millimetres at a change in the beam size by a factor of almost 3 and are related to the displacement of the focal waist centre to the geometric focus with an increase in d_0. In addition, one can see that the increase in the beam aperture is accompanied by an increase in the peak plasma density by more than an order of magnitude. In practice, this obviously manifests itself in the increase in the brightness of the plasma channel luminescence and the change in the colour of the beam cross section image (Figs 5e, 5f). The only difference of the model calculation results from the experimentally obtained lateral filament images (Figs 5a – 5d) is that the calculated filament, depending on the beam size, goes beyond the geometric focus by 1 – 2 cm (it is indicated by a vertical dashed line), whereas this effect was not observed in the experiments. Nevertheless, if we carry out calculations for the filamentation region limited, as previously, by the focal-waist centre ($z = f$), the calculated filament length will correlate with the experimental data in Fig. 6. The corresponding calculated parameter L_{fil}, averaged over three different beams, is shown in Fig. 7 by a solid line.

5. Conclusions

Our experimental data and results of theoretical simulation answer the question formulated in the Introduction: does the length of femtosecond laser filament depend on the initial beam size and, if yes, in which way? We convincingly showed the existence of this dependence for pulsed gigawatt beams of millimetre diameter, propagating in air in the single-filamentation regime. In turn, the character of this dependence is determined by the degree of the focusing of the initial radiation. Physically, the properties revealed are mainly caused by diffraction, the role of which during self-focusing increases with an increase in the beam size.

For example, when a beam is softly focused or collimated, the coordinate of the filament start point moves apart from the beginning of the path with an increase in the beam radius. For relatively wide beams ($R_0 > 2$ mm), the filament loses continuity, and its total length decreases with a rise in the beam radius. The filament length for submillimetre beams, vice versa, increases with an increase in R_0, and the filament remains continuous.

Tightly focused radiation demonstrates other proeprties. In this case, we established (for at least two wavelengths) an effect that has not been mentioned in the literature: the observed filament length depends very weakly on the beam diameter, provided that the peak intensity remains the same. This property is observed for beams up to $R_0 \leqslant 7$ mm in diameter; it does not follow from the formulas of stationary self-focusing theory and is explained mainly by the linear character of the transverse beam compression before the filamentation onset.

When estimating the self-focusing length, the filament start point is generally associated with the point of transverse beam collapse. However, this approach cannot be used for tightly focused beams. It fits well for only not very narrow collimated beams, a case where beam compression is mainly caused by self-focusing and the coordinates of the filament start point and the beam collapse point are close. In the case of sharp focusing, the nonlinearity barely manifests itself in the pre-filamentation stage, and the beam is compressed according to the linear-optics laws.

Acknowledgements. This work was supported by the Fundamental Research Programme 'Extreme Light Fields and Their Applications' of the Presidium of the Russian Academy of Sciences, Integration Project No. 67 of the Presidium of the Siberian Branch of the Russian Academy of Sciences and the Russian Foundation for Basic Research (Grant No. 12-05-00716-a).

References

1. Shen Y.R., Boyd R.W., Lukishova S.G. (Eds) *Self-focusing: Past and Present* (New York: Springer, 2009).

2. Berge L., Skupin S., Nuter R., Kasparian J., Wolf J.-P. *Rep. Prog. Phys.*, **70**, 1633 (2007).
3. Couairon A., Myzyrowicz A. *Phys. Rep.*, **441** (2-4), 47 (2007).
4. Kandidov V.P., Shlenov S.A., Kosareva O.G. *Kvantovaya Elektron*., **39** (3), 205 (2009) [*Quantum Electron*., **39** (3), 205 (2009)].
5. Luo Q., Yu J., Hosseini A., Liu W., Ferland B., Roy G., Chin S.L. *Appl. Opt.*, **44** (3), 391 (2005).
6. Couairon A. *Appl. Phys. B*, **76**, 789 (2003).
7. Brodeur A., Chien C.Y., Ilkov F.A., Chin S.L., Kosareva O.G., Kandidov V.P. *Opt. Lett.*, **22** (5), 304 (1997).
8. Talebpour A., Petit S., Chin S.L. *Opt. Commun.*, **171** (4-6), 285 (1999).
9. Kosareva O.G., Liu W., Panov N.A., Bernhardt J., Ji Z., Sharifi M., Li R., Xu Z., Liu J., Wang Z., Ju J., Lu X., Jiang Y., Leng Y., Liang X., Kandidov V.P., Chin S.L. *Laser Phys.*, **19** (8), 1776 (2009).
10. Loriot V., Hertz E., Faucher O., Lavorel B. *Opt. Express*, **17** (16), 13429 (2009).
11. Geints Yu.E., Kabanov A.M., Zemlyanov A.A., Bykova E.E., Bukin O.A., Golik S.S. *Appl. Phys. Lett.*, **99** (18), 181114 (2011).
12. Perelomov A.M., Popov V.S., Terent'ev M.V. *Zh. Eksp. Tekh. Fiz*., **50**, 1393 (1966).
13. Akhmanov S.A., Vyslouh V.A., Chirkin A.S. *Optics of Femtosecond Laser Pulses* (New York, American Institute of Physics, 1992).
14. Marburger J.H. *Prog. Quantum Electron.*, **4**, 35 (1975).
15. Vlasov S.N., Petrishchev V.A., Talanov V.I. *Radiophys. Quantum Electron.*, **14**, 1353 (1971).
16. Liu W., Luo Q., Théberge F., Xu H.L., Hosseini S.A., Sarifi S.M., Chin S.L. *Appl. Phys. B*, **82** (3), 373 (2006).
17. Geints Yu.E., Zemlyanov A.A. *Opt. Atmos. Okeana*, **23** (4), 274 (2010).
18. Zemlyanov A.A., Geints Yu.E. *Opt. Spektrosk*., **104** (5), 852 (2008).
19. Bukin O.A., Bykova E.E., Geints Yu.E., Golik S.S., Zemlyanov A.A., Il'in A.A., Kabanov A.M., Matvienko G.G., Oshlakov V.K., Sokolova E.B. *Opt. Atmos. Okeana*, **24** (5), 351 (2011).
20. Xu H.L., Azarm A., Bernhardt J., Kamali Y., Chin S.L. *Chem. Phys.*, **360**, 171 (2009).
21. Mizrahi V., Shelton D.P. *Phys. Rev. Lett.*, **55** (7), 696 (1985).
22. Fedorov V.Yu., Kandidov V.P. *Opt. Spektrosk*., **105**, 306 (2008).
23. Geints Yu.E., Zemlyanov A.A. *Kvantovaya Elektron*., **40** (2), 121 (2010) [*Quantum Electron*., **40** (2), 121 (2010)].